A MOLECULAR SIMULATION STUDY OF ADSORPTION OF NITROGEN AND METHANE IN TITANIUM SILICATE (ETS-4)

Flor R. Siperstein[a], Martin Lísal[b,c]* and John K. Brennan[d]

[a] *School of Chemical Engineering & Analytical Science, The University of Manchester, PO Box 88, Sackville Street, Manchester M60 1QD, UK; e-mail: flor.siperstein@manchester.ac.uk*

[b] *E. Hála Laboratory of Thermodynamics, Institute of Chemical Process Fundamentals, Academy of Sciences of the Czech Republic, v.v.i., Rozvojová 135, 165 02 Prague 6-Suchdol, Czech Republic; e-mail: lisal@icpf.cas.cz*

[c] *Department of Physics, Faculty of Science, J. E. Purkinje University, 400 96 Ústí nad Labem, Czech Republic*

[d] *U.S. Army Research Laboratory, Weapons and Materials Research Directorate, Aberdeen Proving Ground, MD 21005-5066, USA; e-mail: john.k.brennan@us.army.mil*

Received August 17, 2009
Accepted October 6, 2009
Published online February 16, 2010

Dedicated to Professor Ivo Nezbeda on the occasion of his 65th birthday.

Adsorption isotherms of methane and nitrogen in porous titanium silicate ETS-4 (Engelhard titanium silicate) are calculated using grand canonical Monte Carlo (GCMC) simulations. Self-diffusion coefficients are determined using molecular dynamics (MD) simulations. Properties for pure gases were determined for two of the ideal ETS-4 polymorphs (ABAB-AA and ABAB-AC) dehydrated at different temperatures (423 and 573 K), taking into account only the framework atoms of the structure and ignoring the non-framework cations and water molecules. It was observed that equilibrium properties are slightly dependent on the structure selected for idealized polymorphs. However, it is not sufficient to explain the differences in adsorption capacity observed experimentally, which can only be explained with the combination of two polymorphs. In polymorphs with straight channels, self-diffusion in the direction of the main channel is two orders of magnitude larger than through the small rings that connect the main channels with some small cages. The trends observed in the self-diffusion coefficient with loading confirmed that crossing an eight-membered ring is an activated process.

Keywords: Adsorption isotherms; ETS-4; Grand canonical Monte Carlo; Molecular dynamics; Self diffusion.

The development of separation systems that are robust and economical, as well as finding suitable sorbents for carbon dioxide–methane and nitrogen–methane separations has been identified as one of the issues to be ad-

doi:10.1135/cccc2009102

dressed for separations research in the 21st century[1]. Nitrogen–methane separations are important to increase the methane content in streams obtained from reservoirs that contain high levels of naturally occurring nitrogen, those obtained from nitrogen injection through enhanced gas recovery[2] or from landfill gases[3].

Even when the nitrogen content in natural gas or landfill gases is considerably lower than the CO_2 content, it is estimated that the cost of separating nitrogen from methane is five times larger than the cost of separating carbon dioxide from methane. Upgrading the methane content in such streams is only economically viable when natural gas prices are high enough[4]. Therefore, understanding the fundamentals of nitrogen–methane separations may provide some direction for the development of adsorbents or processes to reduce the cost of this type of separation.

Separation of carbon dioxide from methane can be achieved through different adsorption-based technologies, such as pressure swing adsorption (PSA) or temperature swing adsorption (TSA)[2]. Carbon dioxide is adsorbed preferentially to methane in zeolites with a high content of non-framework cations, due to the interactions between non-framework cations and the CO_2 quadrupole moment. Therefore it can be assumed that large quadrupole moment of carbon dioxide is the driving force for this separation. The quadrupole moment of nitrogen is considerably smaller than that of carbon dioxide, and insufficient to drive the separation from methane in the same type of zeolites.

Probably the difficulty faced in nitrogen–methane separation is the similar overall behavior of both gases in most zeolites, even though their behavior is a consequence of different phenomena: methane has higher polarizability than nitrogen, and its first non-zero polar moment is the octupole moment, while nitrogen has a non-zero quadrupole moment and smaller polarizability. In general, methane adsorption is more favorable than nitrogen adsorption, but it is assumed that adsorbent heterogeneity or the presence of electric field gradients may favor the adsorption of nitrogen.

Recently, it has been shown that it is possible to tune the pore size of strontium-exchanged titanium silicates with a precision of 0.1 Å [5], and that such materials can be successfully used for nitrogen–methane separations[6]. Other materials that have been proposed for nitrogen–methane separations are ion-exchanged clinoptilolites[7–9]. It has been suggested that the principle of operation of both adsorbents is similar. Depending on the ion-exchange and/or dehydration temperature, the porous network blocks or significantly reduced the entrance of methane, while nitrogen, that has a smaller size, is

able to travel through the porous network. The dehydration temperature refers to the temperature at which the material is "dried" after the synthesis.

In this work, we study adsorption and diffusion of pure nitrogen and methane on different models for ETS-4 in order to understand the molecular mechanisms that allow the preferential adsorption of one gas over the other. In particular, we are interested in showing that the separation can be achieved even in the hypothetical absence of non-framework cations. The separation is mainly driven by the structure of the ETS-4 framework. In general, we observed that nitrogen was better adsorbed in the structures studied. We show that the modification in the structure of ETS-4 upon dehydration does not prevent methane to enter the straight pores in ETS-4, but that it reduces or eliminates the diffusion through the eight-membered ring.

METHODOLOGY

Fluid Model

Methane was considered as a single Lennard–Jones sphere, while nitrogen was modeled as a two-center Lennard–Jones fluid. The interaction parameters for pure methane reproduce well the second virial coefficient[10], and the interaction parameters for nitrogen correctly describe the vapor–liquid equilibrium properties[11]. Despite the fact that the model for nitrogen developed by Vrabec et al.[11] takes into account quadrupole interactions (not taken into account in this work), the potential was not modified because we consider that quadrupole contributions are less important than in bulk nitrogen. We are not considering any explicit charge in the framework atoms or non-framework cations, and the number of nearest neighbors is decreased in confinement compared with the bulk. Interaction parameters for these fluids are summarized in Table I. Mixed interaction parameters were calculated using the Lorentz–Berthelot combining rules.

Solid Model

ETS-4 is a mixed oxide microporous material, essentially a synthetic analogue of the mineral zorite[12,13]. It consists of -O-Ti-O- chains in the [010] direction, whic are connected by silica tetrahedra in the [001] direction and by titanosilicate bridging units in the [100] direction. The bridging unit consists of a five-coordinated titanium atom[14], which is bonded to four silicate tetrahedra and to an apical oxygen atom.

Both ETS-4 and zorite are disordered crystalline materials faulted in the [100] and [001] directions. Their structure can be described as a superposition of four pure polymorphs. In the [100] direction, the bridging units can be stacked in either ABAB- or ABCD-type sequence, whereas in the [001] direction they may be stacked in either an AA- or AC-type arrangement. The faulting in either direction does not block the eight-membered ring pores in the *b* direction, but the faulting in the *c* direction blocks the twelve-membered ring pores[15].

In this work, we constructed different model structures for ETS-4, summarized in Table II. Only the set of polymorphs that are obtained by changing the arrangement of bridging units in the *c* direction from AA- to AC-type arrangement were considered, as this type of faulting yields structures with blocked twelve-membered ring pores. The ABCD-AA and ABCD-AC structures[15] were not considered, as it is assumed that the adsorption properties will be practically the same because the main difference is relative to the location of the twelve-membered ring pores.

TABLE I
Fluid–fluid and fluid–solid interaction parameters

Fluid	σ_{ff}, Å	ε_{ff}/k_B, K	l, Å	σ_{fs}, Å	ε_{fs}/k_B, K
CH_4	3.73	147.95		3.502	104.5
N (from N_2)	3.3211	34.897	1.0464	3.014	85.0

TABLE II
Solid structures used in this work

Model name	Polymorph	Dehydratation temperature, K	Apical TiO
ABAB-AA-423O	ABAB-AA	423	non-blocking
ABAB-AA-573O	ABAB-AA	573	non-blocking
ABAB-AC-423O	ABAB-AC	423	non-blocking
ABAB-AC-573O	ABAB-AC	573	non-blocking
ABAB-AA-423B	ABAB-AA	423	blocking
ABAB-AA-573B	ABAB-AA	573	blocking

All the frameworks used in this work have the same composition because non-framework cations were not taken into account. It is important to point out that the occupancy is less than unity for some framework atoms in the unit cell. In order to construct the smallest *simulation cell* that contains any idealized polymorph, it is necessary to use four unit cells, one in the *a* direction and two in the *b* and *c* directions. The framework composition of the *simulation cell* was $Ti_{16}Si_{48}O_{152}(TiO)_4$. Images of an ABAB-AA structure shown in Fig. 1 correspond to those reported by Kuzinski et al.[5]. The composition of the simulation unit cell is four times the framework composition of a NaSr-ETS-4 structure reported by Nair et al.[14].

It is important to note that in the structure shown in Fig. 1, the apical TiO unit blocks the eight-membered rings preventing diffusion to take place in the *b* direction. Considering that several positions are reported for the apical TiO unit, adsorption equilibrium and diffusion were calculated mainly in model structures where the apical TiO was not the eight-membered ring. We denote with an "O" the structures where the eight-member ring is not blocked by the apical TiO, and with a "B" when it is blocked. Figure 2 shows a modified framework structure with the same cell composition, where TiO units block only the eight-membered rings in the lower part of the box, leaving open for diffusion the rings in the upper part of the box.

For all the sample materials, a grid containing information on the solid–fluid interaction potential at each grid node was pretabulated over one simulation unit cell (four unit cells: one in the a direction, and two in the

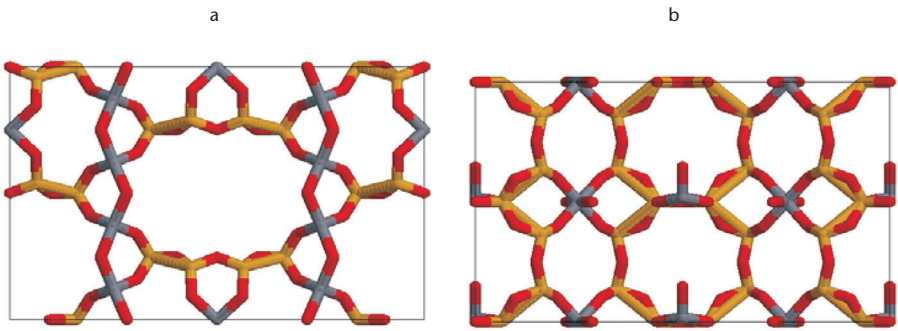

FIG. 1
ETS-4 structures showing: a the straight pores that run along the *c*-direction and b the eight-membered rings that connect the straight pores in the *b*-direction, partially blocked by an apical TiO

b and *c* directions). Hereafter, this box will be referred to simulation unit cell, and the unit cell as one quarter of the simulation unit cell. The framework atoms in the simulation unit cell were selected to reproduce the *ab* and *ac* faults using the information on fractional occupancy of the atoms[16].

The frameworks were assumed to be rigid in the course of the simulation. It is known that the framework flexibility can be important in the determination of transport properties of molecules through such tight passages[17]. In this work we neglect the framework flexibility, assuming that diffusion through some rings may be possible even when it is not observed in a rigid framework.

Fluid–Solid Interactions

Only dispersion–repulsion interactions were taken into account in this work; ion–quadrupole, or ion induction interactions were not considered. It has been recently pointed out that the interaction of non-framework cations with adsorbed non-polar molecules is important for correct description of the behavior of adsorbed molecules and that, depending on the case, cation mobility can play an important role in the shape of the adsorption isotherm[18–20]. Assuming that the framework structure is the most important factor for the ETS-4 sieving properties in nitrogen–methane separations, it is considered that the description of the volume accessible to the adsorbates is more important than the details of the interactions.

Lennard–Jones-type interactions between framework oxygen atoms and fluid molecules were considered:

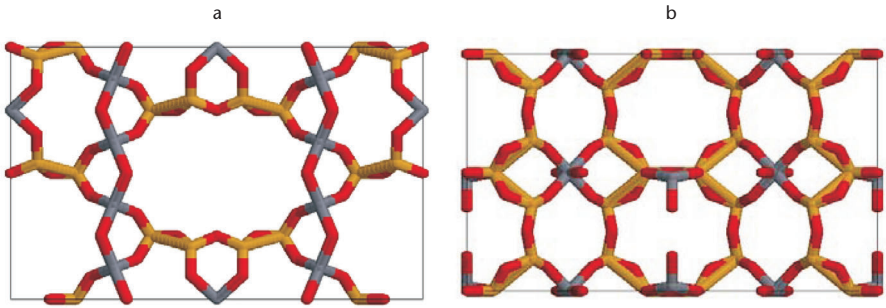

FIG. 2
Modified ETS-4 structures showing: a the straight pores that run along the *c*-direction, b the bottom eight-membered rings blocked by apical TiO units and the top eight-membered rings open and able to connect the straight pores in the *b*-direction

$$u_{ij} = 4\varepsilon_{ij}\left[\left(\frac{\sigma_{ij}}{r_{ij}}\right)^{12} - \left(\frac{\sigma_{ij}}{r_{ij}}\right)^{6}\right] \quad (1)$$

where r_{ij} is the distance between the Lennard–Jones center of an adsorbed molecule *i* and a solid atom *j*, ε_{ij} and σ_{ij} are, respectively, the well-depth and collision diameter of the Lennard–Jones potential between an adsorbed molecule *i* and a solid atom *j*.

Interactions between the adsorbed molecules and the Si and Ti atoms were not considered. It is customary to use effective interactions for oxygen atoms in zeolites that will also account for the interactions with the silicon atoms because it is considered that silicon atoms are not accessible to adsorbed molecules. We use the same assumption even when it is possible for some titanium atoms to be accessible to adsorbed molecules.

It has been shown that several combinations of ε and σ can reproduce the adsorption isotherm of simple gases in silicalite within experimental error[21]. The parameters used in this work are summarized in Table I; different sets of parameters available in the literature were also tested[22–25]. In general, the parameters used and most parameters available in the literature[22,23], give practically the same results, but significant deviations are observed when using the methane-oxygen interaction parameters proposed by Goodbody[25], in which the collision diameter for methane–oxygen is smaller than in the other models.

The methane–oxygen and nitrogen–oxygen interaction parameters selected for this work reproduce well the experimental adsorption isotherm of these gases in silicate[26]. Considering that adsorption of methane in silicalite is more favorable than adsorption of nitrogen, these interaction parameters are useful for testing the influence of the framework structure on the adsorption selectivity.

We do not use the interaction parameters for methane-titanium silicates available in the literature[27] because they strongly overestimate the fluid–solid interactions, yielding heats of adsorption approximately three times larger than those observed experimentally[28,29]. We also did not consider the interaction parameters used in simulations of other porous titanosilicates[30] as they were developed for the determination of the location of non-framework cations and adsorbed water molecules where the most important interactions are Coulombic.

The solid–fluid interaction potential in grand canonical Monte Carlo (GCMC) simulations, and the force in molecular dynamics (MD) simulations, were pretabulated in a grid prior to the simulations. The spacing be-

tween grid points was approximately 0.1 Å. During the simulations, the potential energy or the force of any adsorbed molecule was mapped to the simulation unit cell where pretabulated data was available. A linear interpolation between grid points was performed to determine the potential energy at any point in the box.

Adsorption Isotherms

Adsorption isotherms and heats of adsorption were determined using GCMC simulations following standard procedures[31], where insertion, deletion, translation and rotation in the case of N_2 molecules were considered. For these simulations, it was necessary to add four dummy atoms to the simulation unit cell to block some regions where insertions could be successful, but consist of blocked regions not accessible to molecules diffusing in the main network. These regions correspond to small cages between eight-membered rings that are blocked by an apical TiO unit. In order to identify these regions, a potential energy map was generated, and unconnected regions were identified.

Typical simulations were carried out over 8 simulation unit cells (2×2×2), which correspond to 32 unit cells. Simulations consisted in 200,000 moves for equilibration, and up to 400×10^6 moves for collecting properties. At a given chemical potential (or bulk pressure) we calculated the total number of adsorbed molecules as well as the differential enthalpy of adsorption.

In the course of the simulation, several maps were created to identify the regions where adsorbed molecules are most likely to be found. We identified two main adsorption regions: (i) straight channels and (ii) cavities between two eight-membered rings that connect two adjacent straight channels.

Self-Diffusion

We employed a standard constant-temperature constant-volume (NVT) MD method[31,32] to simulate particle movements through time space. The equations of motion in the NVT MD method were solved using the leap-frog algorithm[32] and by implementing the damped force method of Brown and Clark[33,34] along with the Berendsen thermostat[35] to maintain constant temperature T. A time step of Δt = 2.5 fs and a coupling time constant τ_T = 0.01 ps in the Berendsen thermostat were used for a total simulation time of 10 ns following an equilibration period.

In the course of the NVT MD simulation, we evaluated mean-square displacements in *x*-, *y*- and *z*-directions, denoted as MSD_α, where $\alpha = (x, y, z)$. MSD_α values were used to calculate self-diffusion coefficients in one dimension, D_α, by means of the Einstein equation[32], where

$$D_\alpha = \lim_{t\to\infty} \frac{MSD_\alpha}{2t} \tag{2}$$

and

$$MSD_\alpha = \langle \Delta\alpha(t) \rangle = \left\langle \frac{1}{N} \sum_{j=1}^{N} |\alpha_j(t) - \alpha_j(0)|^2 \right\rangle . \tag{3}$$

In Eqs (*2*) and (*3*), *t* is the time, α_j is a component of the unfolded position of a molecule *j* (not subject to periodic boundary conditions) and $\langle\ \rangle$ means the appropriate ensemble average.

RESULTS AND DISCUSSION

When calculating the potential grid over the simulation unit cell, it is possible to map the accessible sites for an adsorbed molecule. A series of maps for the ABAB-AA-423O and ABAB-AA-573O, in planes that correspond to a constant value in the *x*-direction (half of the simulation unit cell), are shown in Fig. 3. The color code is generated using a scale between zero and unity, which corresponds to the minimum between unity and $\exp(-\beta U)$ at any point in the plane. Therefore, values of zero correspond to non-accessible sites, while values of unity correspond to favorable adsorption sites.

Maps obtained for methane show a clear straight pore, and small cages which appear to be isolated from the straight pore. These small cages are located between two eight-membered rings. For methane to access these cages, a possibility of crossing the eight-membered rings must be assumed, even though the barrier seems high enough to forbid this to happen. It is possible that if one considers lattice vibrations, the barrier to crossing the eight-membered ring should be lower than in the case of rigid frameworks. In this work we assumed that methane could cross the eight-membered rings in the ABAB-AA-423O frameworks, although two scenarios were used to calculate the adsorption isotherm in the ABAB-AA-573O structure: (i) considering that methane could cross the eight-membered rings, and (ii) considering that the small cages are not accessible to methane. In the

latter case, dummy molecules were placed in the cages to avoid insertion of molecules during the GCMC simulations. This is equivalent to the "B" blocked structures.

The maps obtained for a single Lennard–Jones sphere with the properties of nitrogen in Table I show that diffusion in the *y*-direction is possible for nitrogen in ABAB-AA-423O structure. The map obtained for the ABAB-AA-573O structure is similar to those obtained for methane. In the case of nitrogen, it was always assumed that the molecules could cross the eight-membered rings and that all favorable adsorption sites were accessible.

In the cases where all eight-membered rings are partially blocked by one TiO unit, there is no possibility of diffusion in the *y*-direction, as every pore in the *z*-direction is completely isolated from other pores, as shown in

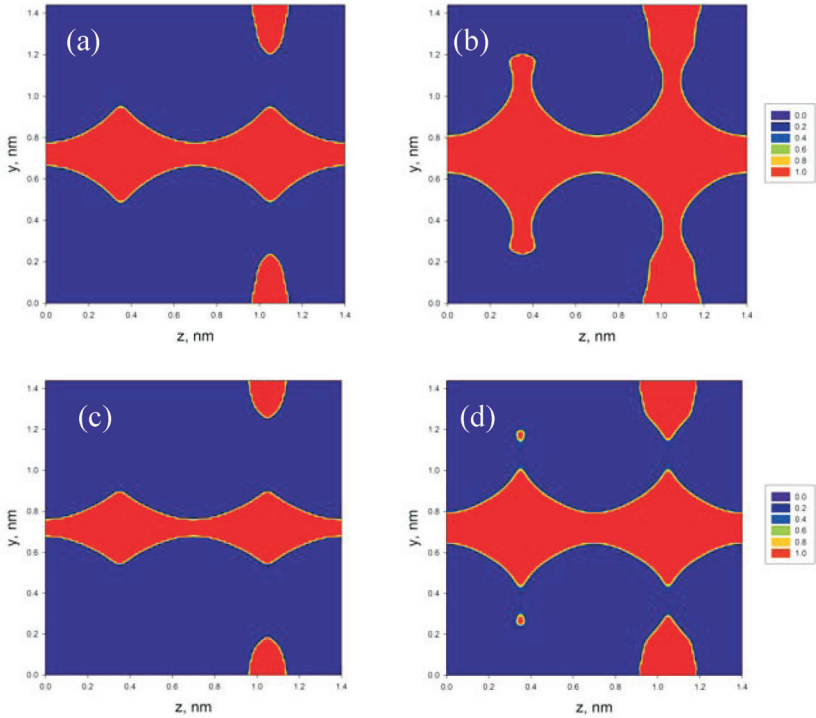

FIG. 3
Accessible sites in a plane x = 1.151 nm for pore model ABAB-AA-423O (a, b) and ABAB-AA-573O (c, d): a and c correspond to methane, and b and d are obtained using a single Lennard–Jones sphere of the nitrogen model in Table I

Fig. 4, and the small cages observed previously are blocked by the apical TiO unit. Only adsorption equilibrium properties were calculated in blocked structures for comparison with open structures, but no MD simulations were performed. Even when molecules cannot pass through the eight-membered rings, the difference in shape of the pores and the larger accessible volume are sufficient to allow nitrogen to be favorably adsorbed.

Finally, a set of potential energy maps for methane and nitrogen in ABAB-AC-423O structures are shown in Fig. 5. For clarity, two simulation cells are shown in the *z*-direction. In the ABAB-AC structures, bridging units block the channels that run in the *z*-direction and only small sections of such channels are accessible to adsorbed molecules. For methane, the accessible regions are unconnected, as shown in Fig. 5a, while clear connec-

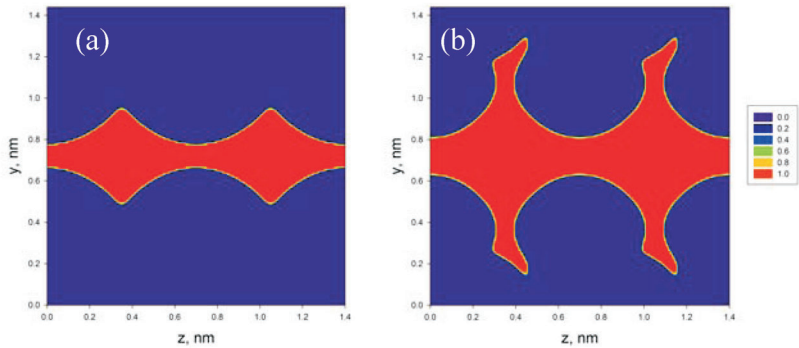

FIG. 4
Accessible sites in a plane x = 1.151 nm for pore model ABAB-AA-423B: a using the methane–oxygen interaction parameters and b using a single Lennard–Jones sphere of the nitrogen model in Table I

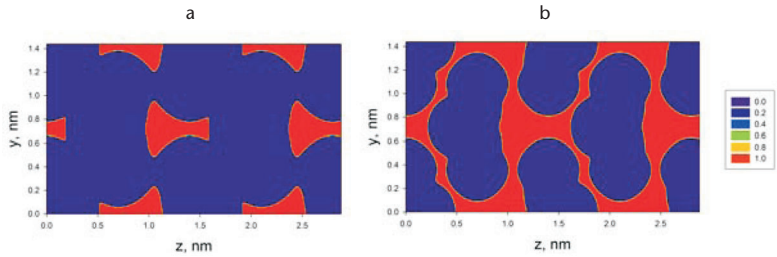

FIG. 5
Accessible sites in a plane x = 1.151 nm for pore model ABAB-AC-423O: a using the methane–oxygen interaction parameters and b using a single Lennard–Jones sphere of the nitrogen model in Table I

tions between the channels in the *z*-directions are observed for nitrogen. Maps for methane and nitrogen in the ABAB-AC-573O structure are similar to those for methane in ABAB-AC-423O (not shown). An assumption that the gases cannot pass through the eight-membered rings would yield the same results as the rings blocked with the apical TiO.

Figures 6 and 7 show equilibrium adsorption isotherms for methane and nitrogen in different structures. In these figures, the amount adsorbed is shown as molecules per unit cell, which corresponds to 1/32th of the actual number of molecules in the simulation box.

For all the structures studied, adsorption of nitrogen is stronger than adsorption of methane. For these simulations we observed consistently lower loadings in the ABAB-AC polymorphs for both gases, which can be due to a different shape of the accessible volume. In general, if we assumed that the small cages between the eight-membered rings are accessible, we observe in structures dehydrated at higher temperatures, higher loadings at low pressures, but a small reduction in the total accessible volume is observed at high pressures, when compared to structures dehydrated at low temperature. This phenomenon is not observed experimentally, where a reduction in loading is found at all pressures upon increasing dehydration temperature. From a theoretical point of view, obtaining higher loadings at low pressures in ABAB-AA-573O structures can be easily explained by the reduction in the pore size of the material, allowing stronger interactions of the adsorbed molecule with the framework. Only a decrease of the whole isotherm in structures dehydrated at high temperatures can be obtained if it is assumed that molecules are not able to cross the eight-membered rings (like in structure ABAB-AA-573B). The amount adsorbed in the small cages amounts up to 30% of the total amount adsorbed.

Figure 8 shows a comparison of the calculated adsorption isotherms with those reported experimentally by Farooq[28,29] The calculated isotherms using very simplified models for the fluid and solid structure, without adjusting any interaction parameter, fall within the correct order of magnitude of the measured adsorption isotherms. Nevertheless, the experimentally measured adsorption isotherms for a sample dehydrated at a low temperature have higher loadings than the isotherms obtained in our simulations for an equivalent material. These differences may be reduced if we take into account the presence of the non-framework cations, as the dispersion forces would be larger and confinement could be stronger. Experimental differential enthalpies of adsorption in all cases were close to 20 kJ/mol [28], and in most cases a slight increase with coverage was observed due to adsorbate–adsorbate interactions. However, for nitrogen in ABAB-AA-423O and

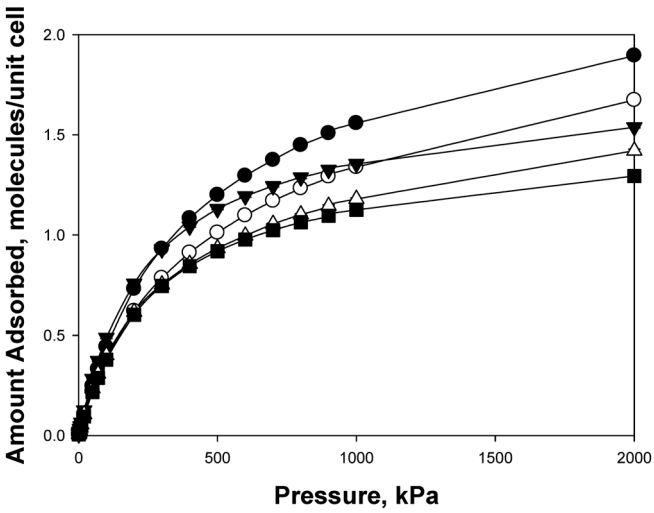

FIG. 6
Methane on ABAB-AA (full symbols) and ABAB-AC (open symbols) polymorphs. Circles, dehydrated at 423 K; triangles, dehydrated at 573 K; squares, ABAB-AA-573B

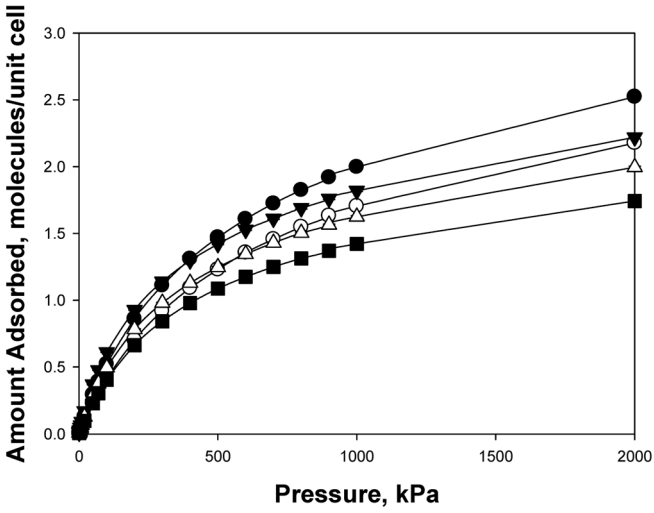

FIG. 7
Nitrogen on ABAB-AA (full symbols) and ABAB-AC (open symbols) polymorphs. Circles, dehydrated at 423 K; triangles, dehydrated at 573 K; squares, ABAB-AA-573B

ABAB-AA-573O, a *u*-shape curve is observed, with a minimum at approximately 1 molecule per unit cell, which indicates that these materials are heterogeneous for nitrogen adsorption.

The decrease in the amount adsorbed, considered only as the decrease in accessible volume of the small cages between the eight-membered rings, is smaller than that observed experimentally. Kuznicki et al.[5] reported even a larger reduction in adsorption capacity with increasing dehydration temperatures. These phenomena cannot be explained using a single polymorph to describe ETS-4, but can be easily understood if the material is described as a combination of polymorphs, where significant regions of the pore net-

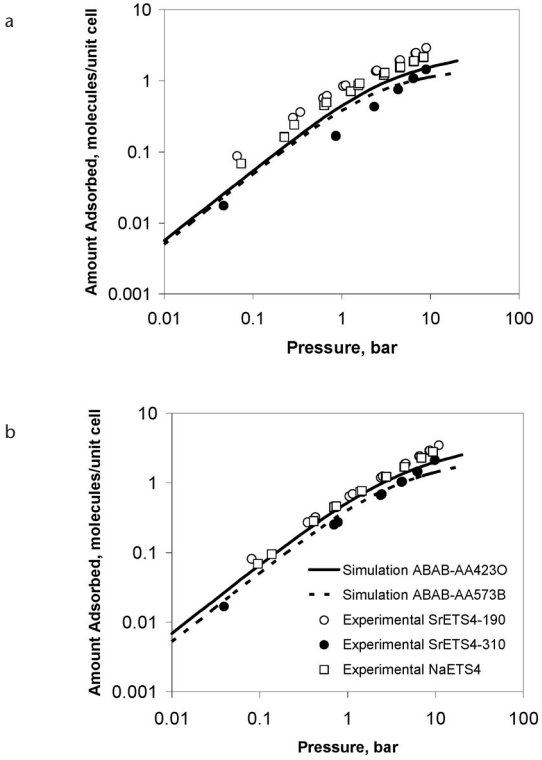

FIG. 8
Comparison of measured adsorption isotherms (symbols) and simulation results (lines) for methane (a) and nitrogen (b). Sr-ETS-4 dehydrated at 463 K (○), Sr-ETS-4 dehydrated at 593 K (●), Na-ETS-4 dehydrated at 593 K (□); simulation on ABAB-AA423O (——), simulation on ABAB-AA573B (- - -), where the volume between two eight-membered rings is not accessible

work are accessible only through the eight-membered rings. This is schematically illustrated in Fig. 9, where the accessible regions for adsorbed molecules are shown in gray and the bridging units as white circles. The cages between two eight-membered rings, are shown as gray circles. The first scheme represents a polymorph of the type ABAB-AA, while the latter represents a mixture of ABAB-AA and ABAB-AC polymorphs. In the ABAB-AA polymorphs, there are no diffusion barriers that limit the access to any straight channel, but in the mixed polymorph material, the region shown with gray lines is accessible only through eight-member rings. The decrease in the amount adsorbed may indicate the total volume occupied by the regions that are accessible only through eight-membered rings.

Of GCMC simulations, we interpret the difference in the reduction of the adsorbed amount reported in the literature[5,28,29] as related to different combinations of the polymorphic structures and difficulty crossing the eight-membered rings for the molecules to access some of the regions of the pore network. In the rest of this paper we analyze MD simulations results for both gases in different structures. Unfortunately, with the selected model for methane, no diffusion was observed through the eight-membered rings for any of the structures studied.

MD simulations show that only diffusion in the *y*-direction is observed for nitrogen adsorbed in the ABAB-AA-423O and ABAB-AC-423O structures

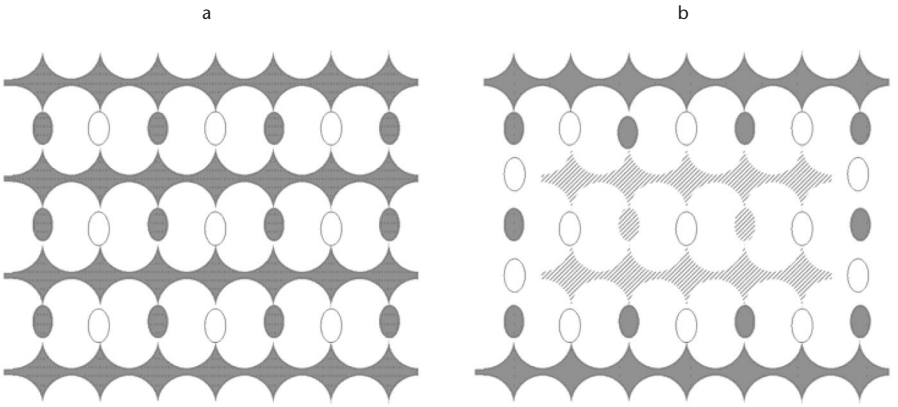

FIG. 9
Schematic representation of a pure polymorph of the type ABAB-AA (a) and a mixed polymorph (b), where the faults create regions of the pore network that are accessible only through the eight-membered rings. In both diagrams, accessible regions are in gray, bridging units are white circles. For the mixed polymorph, the region accessible only through eight-membered rings is shown with dashed lines

(Fig. 10). In order to observe diffusion of methane in the *y*-direction, a flexible framework would be needed, or a different description of methane.

In the ABAB-AA-423O structure (Fig. 10a), which has unblocked straight pores in the *z*-direction, D_z for nitrogen decreases with loading as expected, but D_y increases with loading. D_y is two orders of magnitude smaller than

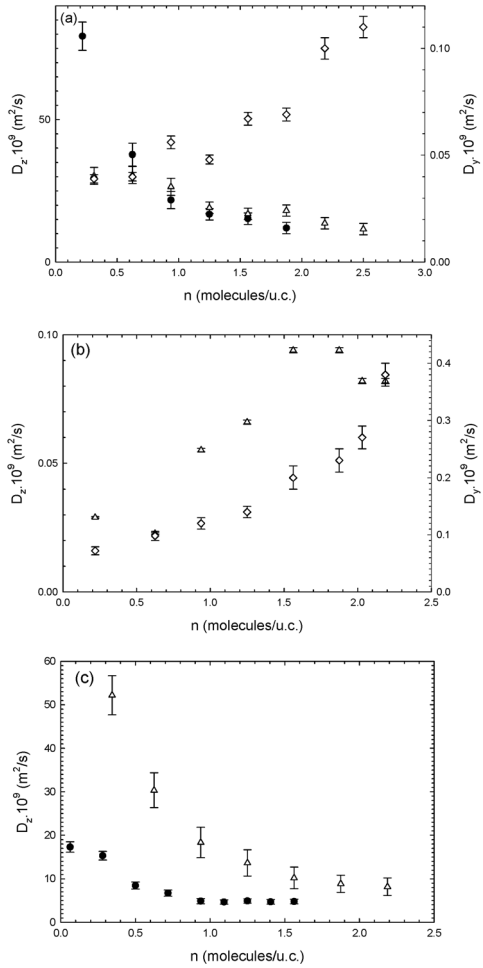

FIG. 10
Self-diffusion coefficients in the *y*- and *z*-directions for nitrogen (◇ and △, respectively) and methane (●) for different structures: ABAB-AA-423O (a), ABAB-AC-423O (b) and ABAB-AA-573O (c)

D_z, and the increase in D_y with loading can be interpreted as the signature of an activated process, where it is more likely to observe a jump in the *y*-direction when the loading in the pore network is higher. At even higher loadings, one would expect D_y to decrease. In the ABAB-AA-573O structure (Fig. 10c), only diffusion in the *z*-direction is observed, which decreases with loading, is observed for both gases.

In the ABAB-AC-423O structure, only diffusion of nitrogen was observed (Fig. 10b). Judging from the maps shown in Fig. 5, no diffusion is expected for methane in the rigid-framework model. It is not only interesting that both D_z and D_y increase with loading, thus indicating the presence of an activated process in both direction, but it must be pointed out that D_y is an order of magnitude larger than D_z. The interpretation of this result is easy to understand when inspecting the adsorption density maps in Fig. 11,

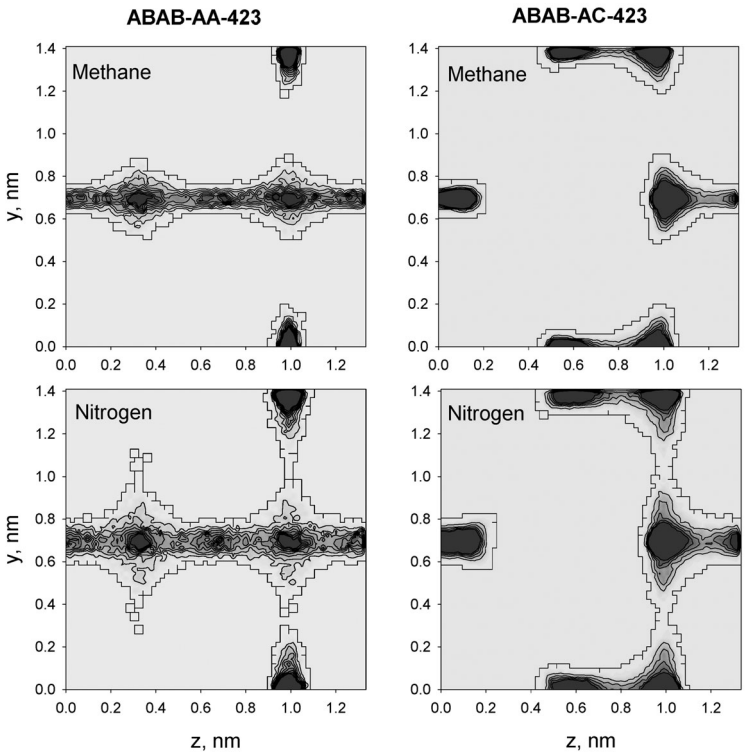

FIG. 11
Density distribution maps in a single pore, obtained by GCMC simulations for methane and nitrogen at 2000 kPa and 300 K. Dark colors indicate regions, where it is more likely to find an adsorbed molecule

where the presence of adsorption sites and transition states can be easily identified. For nitrogen, in the ABAB-AC-423O structure, adsorption sites form practically a straight line in the *y*-direction, bring separated by transition states with lower energy than those in the *z*-direction.

CONCLUSIONS

Simple models represent the ETS-4 capture of most of the features of adsorption of nitrogen and methane. To reproduce properties measured experimentally, it is necessary to describe the material as a combination of at least two polymorphs, where important regions of the pore network are accessible only through eight-membered rings. An increase loading in the self-diffusion coefficients in the *y*-direction confirms that crossing the eight-membered rings is an activated process. Therefore, we suggest that the high selectivity for nitrogen over methane in ETS-4 is mostly due to its framework structure and not to the nature of the non-framework cations. Nevertheless, the presence of non-framework cations can be significant as they may block some of the adsorption sites observed during the GCMC simulations.

It is expected that pores of the size observed in ETS-4, taking into account framework vibrations, should have an important effect on the calculated properties, especially for methane, for which no diffusion in the *y*-direction was observed using the selected models.

Support from the Marie Curie Open Transfer of Knowledge project (MTKD-CT-2005-030040) and a mobility grant from the Generalitat de Catalunya BE00334 are gratefully acknowledged. F. R. Siperstein acknowledges support from the Ramón y Cajal Program of the Spanish Ministerio de Educación y Ciencia and the hospitality at the E. Hála Laboratory of Thermodynamics during this work, as well as useful discussions with F. Leroy at Universitat Rovira i Virgili in Tarragona, Spain. M. Lísal acknowledges the Czech Science Foundation (Grant No. 203/08/0094), by the National Research Programme "Information Society" (Project No. 1ET400720507), by the Grant Programme of the Academy of Sciences of the Czech Republic "Nanotechnology for the Society" (Project No. KAN400720701), and by the European Community under the 6th Framework Programme (Project MULTIPRO No. 033304) and under the 7th Framework Programme (Project COST TD0802). This project was partially funded by HERA AMASA SL and DINAMIC Innovation Centre.

REFERENCES

1. Noble R. D., Agrawal R.: *Ind. Eng. Chem. Res.* **2005**, *44*, 2887.
2. Yang R. T.: *Adsorbents: Fundamentals and Applications*. Wiley Interscience, Hoboken (NJ) 2003.

3. *The Share of Renewable Energy in the EU Country Profiles*. Overview of Renewable Energy Sources in the Enlarged European Union. Commission of the European Communities, Brussels 26/05/2004.
4. Knaebel K. S., Reinhold H. E.: *Adsorption* **2003**, *9*, 87.
5. Kuznicki S. M., Bell V. A., Nair S., Hillhouse H. W., Jacubinas R. M., Braunbarth C. M., Toby B. H., Tsapatsis M.: *Nature* **2001**, *412*, 720.
6. Kuznicki S. M., Bell V. A., Petrovic I., Desai B. T.: U.S. 6,068,682, 2000.
7. Ackley M. W., Yang R. T.: *AIChE J.* **1991**, *37*, 1645.
8. Jayaraman A., Hernandez-Maldonado A. J., Yang R. T., Chinn D., Munson C. L., Mohr D. H.: *Chem. Eng. Sci.* **2004**, *59*, 2407.
9. Jayaraman A., Yang R. T., Chinn D., Munson C. L.: *Ind. Eng. Chem. Res.* **2005**, *44*, 5184.
10. Maitland G. C., Rigby M., Smith E. B., Wakeham W. A.: *Intermolecular Forces: Their Origin and Determination*. Oxford University Press, Oxford 1981.
11. Vrabec J., Stoll J., Hasse H.: *J. Phys. Chem. B* **2001**, *105*, 12126.
12. Cruciani G., De Luca P., Nastro A., Pattison P.: *Microporous Mesoporous Mater.* **1998**, *21*, 143.
13. Philippou A., Anderson M. W.: *Zeolites* **1996**, *16*, 98.
14. Nair S., Jeong H. K., Chandrasekaran A., Braunbarth C. M., Tsapatsis M., Kuznicki S. M.: *Chem. Mater.* **2001**, *13*, 4247.
15. Braunbarth C., Hillhouse H. W., Nair S., Tsapatsis M., Burton A., Lobo R. F., Jacubinas R. M., Kuznicki S. M.: *Chem. Mater.* **2000**, *12*, 1857.
16. Nair S., Tsapatsis M., Toby B. H., Kuznicki S. M.: *J. Am. Chem. Soc.* **2001**, *123*, 12781.
17. Leroy F., Rousseau B., Fuchs A. H.: *Phys. Chem. Chem. Phys.* **2004**, *6*, 775.
18. Maurin G., Llewellyn P., Poyet T., Kuchta B.: *J. Phys. Chem. B* **2005**, *109*, 125.
19. Calero S., Dubbeldam D., Krishna R., Smit B., Vlugt T. J. H., Denayer J. F. M., Martens J. A., Maesen T. L. M.: *J. Am. Chem. Soc.* **2004**, *126*, 11377.
20. Beerdsen E., Smit B., Calero S.: *J. Phys. Chem. B* **2002**, *106*, 10659.
21. Talu O., Myers A. L.: *Colloids Surf., A* **2001**, *187–188*, 83.
22. Smit B.: *J. Phys. Chem.* **1995**, *99*, 5597.
23. Vlugt T. J. H., Zhu W., Kapteijn F., Moulijn J. A., Smit B., Krishna R.: *J. Am. Chem. Soc.* **1998**, *120*, 5599.
24. Dubbeldam D., Calero S., Vlugt T. J. H., Krishna R., Maesen T. L. M., Smit B.: *J. Phys. Chem. B* **2004**, *108*, 12301.
25. Goodbody S. J., Watanabe K., MacGowan D., Walton J. P. R. B., Quirke N.: *J. Chem. Soc., Faraday Trans.* **1991**, *87*, 1951.
26. Dunne J. A., Mariwala R., Rao M., Sircar S., Gorte R. J., Myers A. L.: *Langmuir* **1996**, *12*, 5888.
27. Mitchell M. C., Gallo M., Nenoff T. M.: *J. Chem. Phys.* **2004**, *121*, 1910.
28. Marathe R. P., Mantri K., Srinivasan M. P., Farooq S.: I*nd. Eng. Chem. Res.* **2004**, *43*, 5281.
29. Marathe R. P., Srinivasan M. P., Farooq S.: *Chem. Eng. Sci.* **2004**, *59*, 6021.
30. Larentzos J. P., Clearfield A., Tripathi A., Maginn E. J.: *J. Phys. Chem. B* **2004**, *108*, 17560.
31. Frenkel D., Smit B.: *Understanding Molecular Simulation: From Algorithms to Applications*. Academic Press, London 2002.
32. Allen M. P., Tildesley D. J.: *Computer Simulation of Liquids*. Clarendon Press, Oxford 1987.
33. Brown D., Clarke J. H. R.: *Mol. Phys.* **1984**, *51*, 1243.

34. Fincham D.: *Mol. Simul.* **1992**, *8*, 165.
35. Berendsen H. J. C., Postma J. P. M., van Gunsteren W. F., DiNola A., Haak J. R.: *J. Chem. Phys.* **1984**, *81*, 3684.